

**MACS: AN AGENT-BASED MEMETIC MULTIOBJECTIVE
OPTIMIZATION ALGORITHM APPLIED TO SPACE TRAJECTORY
DESIGN**

Massimiliano Vasile – Federico Zuiani

Space Advanced Research Team, University of Strathclyde

James Weir Building 75 Montrose Street G1 1XJ, Glasgow, United Kingdom

massimiliano.vasile@strath.ac.uk, f.zuiani@aero.gla.ac.uk

ABSTRACT

This paper presents an algorithm for multiobjective optimization that blends together a number of heuristics. A population of agents combines heuristics that aim at exploring the search space both globally and in a neighborhood of each agent. These heuristics are complemented with a combination of a local and global archive. The novel agent-based algorithm is tested at first on a set of standard problems and then on three specific problems in space trajectory design. Its performance is compared against a number of state-of-the-art multiobjective optimisation algorithms that use the Pareto dominance as selection criterion: NSGA-II, PAES, MOPSO, MTS. The results demonstrate that the agent-based search can identify parts of the Pareto set that the other algorithms were not able to capture. Furthermore, convergence is statistically better although the variance of the results is in some cases higher.

KEYWORDS

Multiobjective optimisation; trajectory optimisation; memetic algorithms; multiagent systems.

1. INTRODUCTION

The design of a space mission steps through different phases of increasing complexity. In the first phase, a trade-off analysis of several options is required. The trade-off analysis compares and contrasts design solutions according to different criteria and aims at selecting one or two options that satisfy mission requirements. In mathematical terms, the problem can be formulated as a multiobjective optimization problem.

As part of the trade-off analysis, multiple transfer trajectories to the destination need to be designed. Each transfer should be optimal with respect to a number of criteria. The solution of the associated multiobjective optimization problem, has been addressed, by many authors, with evolutionary techniques. Coverstone et al. [1] proposed the use of multiobjective genetic algorithms for the optimal design of low-thrust trajectories. Dachwald et al. proposed the combination of a neurocontroller and of a multiobjective evolutionary algorithm for the design of low-thrust trajectories [2]. In 2005 a study by Lee et al. [3] proposed the use of a Lyapunov controller with a multiobjective evolutionary algorithm for the design of low-thrust spirals. More recently, Schütze et al. proposed some innovative techniques to solve multiobjective optimization problems for multi-gravity low-thrust trajectories. Two of the interesting aspects of the work of Schütze et al. are the archiving of ϵ - and Δ -approximated solutions, to the known best Pareto front [4], and the deterministic pre-pruning of the search space [5]. In 2009, Delnitz et al. [6] proposed the use of multiobjective subdivision techniques for the design of low-thrust transfers to the halo orbits around the L_2 libration point in the Earth-Moon system. Minisci et al. presented an interesting comparison between an EDA-based algorithm, called MOPED, and NSGA-II on some constrained and unconstrained multi-impulse orbital transfer problems [7].

In this paper, a hybrid population-based approach that blends a number of heuristics is

proposed. In particular, the search for Pareto optimal solutions is carried out globally by a population of agents implementing classical social heuristics and more locally by a subpopulation implementing a number of individualistic actions. The reconstruction of the set of Pareto optimal solutions is handled through two archives: a local and a global one.

The individualistic actions presented in this paper are devised to allow each agent to independently converge to the Pareto optimal set. Thus creating its own partial representation of the Pareto front. Therefore, they can be regarded as memetic mechanisms associated to a single individual. It will be shown that individualistic actions significantly improve the performance of the algorithm.

The algorithm proposed in this paper is an extension of the Multi-Agent Collaborative Search (MACS), initially proposed in [8, 9], to the solution of multiobjective optimisation problems. Such an extension required the modification of the selection criterion, for both global and local moves, to handle Pareto dominance and the inclusion of new heuristics to allow the agents to move toward and along the Pareto front. As part of these new heuristics, this paper introduces a dual archiving mechanism for the management of locally and globally Pareto optimal solutions and an attraction mechanism that improves the convergence of the population.

The new algorithm is here applied to a set of known standard test cases and to three space mission design problems. The space mission design cases in this paper consider spacecraft equipped with a chemical engine and performing a multi-impulse transfer. Although these cases are different from some of the above-mentioned examples, that consider a low-thrust propulsion system, nonetheless the size and complexity of the search space is comparable. Furthermore, it provides a first test benchmark for multi-impulsive problems that have been extensively studied in the single objective case but for which only few comparative studies exist in the multiobjective case [7].

The paper is organised as follows: section two contains the general formulation of the problem, the third section starts with a general introduction to the multi-agent collaborative search algorithm and heuristics before going into some of the implementation details. Section four contains a set of comparative tests that demonstrates the effec-

tiveness of the heuristics implemented in MACS. The section briefly introduces the algorithms against which MACS is compared and the two test benchmarks that are used in the numerical experiments. It then defines the performance metrics and ends with the results of the comparison.

2. PROBLEM FORMULATION

A general problem in multiobjective optimization is to find the feasible set of solutions that satisfies the following problem:

$$\min_{\mathbf{x} \in D} \mathbf{f}(\mathbf{x}) \quad (1)$$

where D is a hyperrectangle defined as $D = \{x_j \mid x_j \in [b_j^l, b_j^u] \subseteq \mathbb{R}, j = 1, \dots, n\}$ and \mathbf{f} is the vector function:

$$\mathbf{f} : D \rightarrow \mathbb{R}^m, \quad \mathbf{f}(\mathbf{x}) = [f_1(\mathbf{x}), f_2(\mathbf{x}), \dots, f_m(\mathbf{x})]^T \quad (2)$$

The optimality of a particular solution is defined through the concept of dominance: with reference to problem (1), a vector $\mathbf{y} \in D$ is dominated by a vector $\mathbf{x} \in D$ if $f_j(\mathbf{x}) < f_j(\mathbf{y})$ for all $j = 1, \dots, m$. The relation $\mathbf{x} \prec \mathbf{y}$ states that \mathbf{x} dominates \mathbf{y} .

Starting from the concept of dominance, it is possible to associate, to each solution in a set, the scalar dominance index:

$$I_d(\mathbf{x}_j) = |\{i \mid i \wedge j \in N_p \wedge \mathbf{x}_i \prec \mathbf{x}_j\}| \quad (3)$$

where the symbol $|\cdot|$ is used to denote the cardinality of a set and N_p is the set of the indices of all the solutions. All non-dominated and feasible solutions form the set:

$$X = \{\mathbf{x} \in D \mid I_d(\mathbf{x}) = 0\} \quad (4)$$

Therefore, the solution of problem (1) translates into finding the elements of X . If X is made of a collection of compact sets of finite measure in \mathbb{R}^n , then once an element

of X is identified it makes sense to explore its neighborhood to look for other elements of X . On the other hand, the set of non dominated solutions can be disconnected and its elements can form islands in D . Hence, restarting the search process in unexplored regions of D can increase the collection of elements of X .

The set X is the Pareto set and the corresponding image in criteria space is the Pareto front. It is clear that in D there can be more than one X_l containing solutions that are locally non-dominated, or locally Pareto optimal. The interest is, however, to find the set X_g that contains globally non-dominated, or globally Pareto optimal, solutions.

3. MULTIAGENT COLLABORATIVE SEARCH

The key motivation behind the development of multi-agent collaborative search was to combine local and global search in a coordinated way such that local convergence is improved while retaining global exploration [9]. This combination of local and global search is achieved by endowing a set of agents with a repertoire of actions producing either the sampling of the whole search space or the exploration of a neighborhood of each agent. More precisely, in the following, global exploration moves will be called collaborative actions while local moves will be called individualistic actions. Note that not all the individualistic actions, described in this paper, aim at exploring a neighborhood of each agent, though. The algorithm presented in this paper is a modification of MACS to tackle multiobjective optimization problems. In this section, the key heuristics underneath MACS will be described together with their modification to handle problem (1) and reconstruct X .

3.1. GENERAL ALGORITHM DESCRIPTION

A population P_0 of n_{pop} virtual agents, one for each solution vector \mathbf{x}_i , with $i = 1, \dots, n_{pop}$, is deployed in D . The population evolves through a number of generations. At every generation k , the dominance index (3) of each agent $\mathbf{x}_{i,k}$ in the population P_k is evaluated. The agents with dominance index $I_d = 0$ form a set X_k of non-dominated solutions. Hence, problem (1) translates into finding a series of sets X_k such that $X_k \rightarrow X_g$ for $k \rightarrow k_{max}$ with k_{max} possibly a finite number.

The position of each agent in D is updated through a number of heuristics. Some are called *collaborative actions* because they are derived from the interaction of at least two agents and involve the entire population at one time. The general collaborative heuristic can be expressed in the following form:

$$\mathbf{x}_k = \mathbf{x}_k + S(\mathbf{x}_k + \mathbf{u}_k)\mathbf{u}_k \quad (5)$$

where \mathbf{u}_k depends on the other agents in the population and S is a selection function which yields 0 if the candidate point $\mathbf{x}_k + \mathbf{u}_k$ is not selected or 1 if it is selected (see Section 3.2). In this implementation a candidate point is selected if its dominance index is better or equal than the one of \mathbf{x}_k . A first restart mechanism is then implemented to avoid crowding. This restart mechanism is taken from [9] and prevents the agents from overlapping or getting too close. It is governed by the crowding factor w_c that defines the minimum acceptable normalized distance between agents. Note that, this heuristic increases the uniform sampling rate of D , when activated, thus favoring exploration. On the other hand, by setting w_c small the agents are more directed towards local convergence.

After all the collaborative and restart actions have been implemented, the resulting updated population P_k is ranked according to I_d and split in two subpopulations: P_k^u and P_k^l . The agents in each subpopulation implement sets of, so called, *individualistic actions* to collect samples of the surrounding space and to modify their current location. In particular, the last $n_{pop} - f_e n_{pop}$ agents belong to P_k^u and implement heuristics that can be expressed in a form similar to Eq. (5) but with \mathbf{u}_k that depends only on \mathbf{x}_k .

The remaining $f_e n_{pop}$ agents belong to P_k^l and implement a mix of actions that aim at either improving their location or exploring the neighborhood $N_\rho(\mathbf{x}_{i,k})$, with $i = 1, \dots, f_e n_{pop}$. $N_\rho(\mathbf{x}_{i,k})$ is a hyperrectangle centered in $\mathbf{x}_{i,k}$. The intersection $N_\rho(\mathbf{x}_{i,k}) \cap D$ represents the local region around agent $\mathbf{x}_{i,k}$ that one wants to explore. The *size* of $N_\rho(\mathbf{x}_{i,k})$ is specified by the value $\rho(\mathbf{x}_{i,k})$: the i^{th} edge of N_ρ has length $2\rho(\mathbf{x}_{i,k}) \max\{b_j^u - x_{i,k}[j], x_{i,k}[j] - b_j^l\}$.

The agents in P_k^l generate a number of perturbed solutions \mathbf{y}_s for each $\mathbf{x}_{i,k}$, with $s =$

$1, \dots, s_{max}$. These solutions are collected in a local archive A_l and a dominance index is computed for all the elements in A_l . If at least one element $\mathbf{y}_s \in A_l$ has $I_d = 0$ then $\mathbf{x}_{i,k} \leftarrow \mathbf{y}_s$. If multiple elements of A_l have $I_d = 0$, then the one with the largest variation, with respect to $\mathbf{x}_{i,k}$, in criteria space is taken. Figure 1(a) shows three agents (circles) with a set of locally generated samples (stars) in their respective neighborhoods (dashed square). The arrows indicate the direction of motion of each agent. The figure shows also the local archive for the first agent A_{l_1} and the target global archive X_g .

The ρ value associated to an agent is updated at each iteration according to the rule devised in [9]. Furthermore, a value $s(\mathbf{x}_{i,k})$ is associated to each agent $\mathbf{x}_{i,k}$ to specify the number of samples allocated to the exploration of $N_\rho(\mathbf{x}_{i,k})$. This value is updated at each iteration according to the rule devised in [9].

The adaptation of ρ is introduced to allow the agents to self-adjust the neighborhood removing the need to set a priori the appropriate size of $N_\rho(\mathbf{x}_{i,k})$. The consequence of this adaptation is an intensification of the local search by some agents while the others are still exploring. In this respect, MACS works opposite to Variable Neighborhood Search heuristics, where the neighborhood is adapted to improve global exploration, and differently than Basin Hopping heuristics in which the neighborhood is fixed. Similarly, the adaptation of $s(\mathbf{x}_{i,k})$ avoids setting a priori an arbitrary number of individualistic moves and has the effect of avoiding an excessive sampling of $N_\rho(\mathbf{x}_{i,k})$ when ρ is small. The value of $s(\mathbf{x}_{i,k})$ is initialized to the maximum number of allowable individualistic moves s_{max} . The value of s_{max} is here set equal to the number of dimensions n . This choice is motivated by the fact that a gradient-based method would evaluate the function a minimum of n times to compute an approximation of the gradient with finite differences. Note that the set of individualistic actions allows the agents to independently move towards and within the set X , although no specific mechanism is defined as in [10]. On the other hand the mechanisms proposed in [10] could further improve the local search and will be the subject of a future investigation. All the elements of X_k found during one generation are stored in a global archive A_g . The elements in A_g are a selection of the elements collected in all the local archives.

Figure 1: Illustration of the a) local moves and archive and b) global moves and archive.

Figure 1(b) illustrates three agents performing two social actions that yield two samples (black dots). The two samples together with the non-dominated solutions coming from the local archive form the global archive. The archive A_g is used to implement an attraction mechanism that improves the convergence of the worst agents (see Sections 3.4.1). During the global archiving process a second restart mechanism that reinitializes a portion of the population (*bubble restart*) is implemented. Even this second restart mechanism is taken from [9] and avoids that, if ρ collapses to zero, the agent keeps on sampling a null neighborhood.

Note that, within the MACS framework, other strategies can be assigned to the agents to evaluate their moves in the case of multiple objective functions, for example a decomposition technique [11]. However, in this paper we develop the algorithm based only on the use of the dominance index.

3.2. COLLABORATIVE ACTIONS

Collaborative actions define operations through which information is exchanged between pairs of agents. Consider a pair of agents \mathbf{x}_1 and \mathbf{x}_2 , with $\mathbf{x}_1 \prec \mathbf{x}_2$. One of the two agents is selected at random in the worst half of the current population (from the point of view of the property I_d), while the other is selected at random from the whole population. Then, three different actions are performed. Two of them are defined by adding to \mathbf{x}_1 a step \mathbf{u}_k defined as follows:

$$\mathbf{u}_k = \alpha r^t (\mathbf{x}_2 - \mathbf{x}_1), \quad (6)$$

and corresponding to: *extrapolation* on the side of \mathbf{x}_1 ($\alpha = -1, t = 1$), with the further constraint that the result must belong to the domain D (i.e., if the step \mathbf{u}_k leads out of D , its size is reduced until we get back to D); *interpolation* ($\alpha = 1$), where a random point between \mathbf{x}_1 and \mathbf{x}_2 is sampled. In the latter case, the shape parameter t is defined

Algorithm 1 Main MACS algorithm

- 1: Initialize a population P_0 of n_{pop} agents in D , $k = 0$, number of function evaluations $n_{eval} = 0$, maximum number of function evaluations N_e , crowding factor w_c
 - 2: **for all** $i = 1, \dots, n_{pop}$ **do**
 - 3: $\mathbf{x}_{i,k} = \mathbf{x}_{i,k} + S(\mathbf{x}_{i,k} + \mathbf{u}_{i,k})\mathbf{u}_{i,k}$
 - 4: **end for**
 - 5: Rank solutions in P_k according to I_d
 - 6: Re-initialize crowded agents according to the single agent restart mechanism
 - 7: **for all** $i = f_e n_{pop}, \dots, n_{pop}$ **do**
 - 8: Generate n_p mutated copies of $\mathbf{x}_{i,k}$.
 - 9: Evaluate the dominance of each mutated copy \mathbf{y}_p against $\mathbf{x}_{i,k}$, with $p = 1, \dots, n_p$
 - 10: **if** $\exists p | \mathbf{y}_p \prec \mathbf{x}_{i,k}$ **then**
 - 11: $\bar{p} = \arg \max_p \|\mathbf{y}_p - \mathbf{x}_{i,k}\|$
 - 12: $\mathbf{x}_{i,k} \leftarrow \mathbf{y}_{\bar{p}}$
 - 13: **end if**
 - 14: **end for**
 - 15: **for all** $i = 1, \dots, f_e n_{pop}$ **do**
 - 16: Generate $s < s_{max}$ individual actions \mathbf{u}_s such that $\mathbf{y}_s = \mathbf{x}_{i,k} + \mathbf{u}_s$
 - 17: **if** $\exists s | \mathbf{y}_s \prec \mathbf{x}_{i,k}$ **then**
 - 18: $\bar{s} = \arg \max_s \|\mathbf{y}_s - \mathbf{x}_{i,k}\|$
 - 19: $\mathbf{x}_{i,k} \leftarrow \mathbf{y}_{\bar{s}}$
 - 20: **end if**
 - 21: Store candidate elements \mathbf{y}_s in the local archive A_l
 - 22: Update $\rho(\mathbf{x}_{i,k})$ and $s(\mathbf{x}_{i,k})$
 - 23: **end for**
 - 24: Form $P_k = P_k^l \cup P_k^u$ and $\hat{A}_g = A_g \cup A_l \cup P_k$
 - 25: Compute I_d of all the elements in \hat{A}_g
 - 26: $A_g = \{\mathbf{x} | \mathbf{x} \in \hat{A}_g \wedge I_d(\mathbf{x}) = 0 \wedge \|\mathbf{x} - \mathbf{x}_{A_g}\| > w_c\}$
 - 27: Re-initialize crowded agents in P_k according to the second restart mechanism
 - 28: Compute attraction component to A_g for all $\mathbf{x}_{i,k} \in P_k \setminus X_k$
 - 29: $k = k + 1$
 - 30: **Termination** Unless $n_{eval} > N_e$, GoTo Step 2
-

as follows:

$$t = 0.75 \frac{s(\mathbf{x}_1) - s(\mathbf{x}_2)}{s_{\max}} + 1.25 \quad (7)$$

The rationale behind this definition is that we are favoring moves which are closer to the agent with a higher fitness value if the two agents have the same s value, while in the case where the agent with highest fitness value has a s value much lower than that of the other agent, we try to move away from it because a small s value indicates that improvements close to the agent are difficult to detect.

The third operation is the *recombination* operator, a *single-point crossover*, where, given the two agents: we randomly select a component j ; split the two agents into two parts, one from component 1 to component j and the other from component $j + 1$ to component n ; and then we combine the two parts of each of the agents in order to generate two new solutions. The three operations give rise to four new samples, denoted by $\mathbf{y}_1, \mathbf{y}_2, \mathbf{y}_3, \mathbf{y}_4$. Then, I_d is computed for the set $\mathbf{x}_2, \mathbf{y}_1, \mathbf{y}_2, \mathbf{y}_3, \mathbf{y}_4$. The element with $I_d = 0$ becomes the new location of \mathbf{x}_2 in D .

3.3. INDIVIDUALISTIC ACTIONS

Once the collaborative actions have been implemented, each agent in P_k^u is mutated a number of times: the lower the ranking the higher the number of mutations. The mutation mechanisms is not different from the single objective case but the selection is modified to use the dominance index rather than the objective values.

A mutation is simply a random vector \mathbf{u}_k such that $\mathbf{x}_{i,k} + \mathbf{u}_k \in D$. All the mutated solution vectors are then compared to $\mathbf{x}_{i,k}$, i.e. I_d is computed for the set made of the mutated solutions and $\mathbf{x}_{i,k}$. If at least one element \mathbf{y}_p of the set has $I_d = 0$ then $\mathbf{x}_{i,k} \leftarrow \mathbf{y}_p$. If multiple elements of the set have $I_d = 0$, then the one with the largest variation, with respect to $\mathbf{x}_{i,k}$, in criteria space is taken.

Each agent in P_k^l performs at most s_{max} of the following individualistic actions: *inertia*, *differential*, *random with line search*. The overall procedure is summarized in Algorithm 2 and each action is described in detail in the following subsections.

3.3.1. Inertia

If agent i has improved from generation $k - 1$ to generation k , then it follows the direction of the improvement (possibly until it reaches the border of D), i.e., it performs the following step:

$$\mathbf{y}_s = \mathbf{x}_{i,k} + \bar{\lambda} \Delta_I \quad (8)$$

where $\bar{\lambda} = \min\{1, \max\{\lambda : \mathbf{y}_s \in D\}\}$ and $\Delta_I = (\mathbf{x}_{i,k} - \mathbf{x}_{i,k-1})$.

3.3.2. Differential

This step is inspired by Differential Evolution [12]. It is defined as follows: let $\mathbf{x}_{i_1,k}$, $\mathbf{x}_{i_2,k}$, $\mathbf{x}_{i_3,k}$ be three randomly selected agents; then

$$\mathbf{y}_s = \mathbf{x}_{i,k} + \mathbf{e} [\mathbf{x}_{i_1,k} + F(\mathbf{x}_{i_3,k} - \mathbf{x}_{i_2,k})] \quad (9)$$

with \mathbf{e} a vector containing a random number of 0 and 1 (the product has to be intended componentwise) with probability 0.8 and $F = 0.8$ in this implementation. For every component $y_s[j]$ of \mathbf{y}_s that is outside the boundaries defining D then $y_s[j] = r(b_j^u - b_j^l) + b_j^l$, with $r \in U(0, 1)$. Note that, although this action involves more than one agent, its outcome is only compared to the other outcomes coming from the actions performed by agent $\mathbf{x}_{i,k}$ and therefore it is considered individualistic.

3.3.3. Random with Line Search

This move realizes a local exploration of the neighborhood $N(\mathbf{x}_{i,k})$. It generates a first random sample $\mathbf{y}_s \in N(\mathbf{x}_{i,k})$. Then if \mathbf{y}_s is not an improvement, it generates a second sample \mathbf{y}_{s+1} by extrapolating on the side of the better one between \mathbf{y}_s and $\mathbf{x}_{i,k}$:

$$\mathbf{y}_{s+1} = \mathbf{x}_{i,k} + \bar{\lambda} [\alpha_2 r^t (\mathbf{y}_s - \mathbf{x}_{i,k}) + \alpha_1 (\mathbf{y}_s - \mathbf{x}_{i,k})] \quad (10)$$

with $\bar{\lambda} = \min\{1, \max\{\lambda : \mathbf{y}_{s+1} \in D\}\}$ and where $\alpha_1, \alpha_2 \in \{-1, 0, 1\}$, $r \in U(0, 1)$ and t is a shaping parameter which controls the magnitude of the displacement. Here we use the parameter values $\alpha_1 = 0$, $\alpha_2 = -1$, $t = 1$, which corresponds to *extrapolation* on the side of $\mathbf{x}_{i,k}$, and $\alpha_1 = \alpha_2 = 1$, $t = 1$, which corresponds to *extrapolation* on the side of \mathbf{y}_s .

The outcome of the extrapolation is used to construct a second order one-dimensional model of I_d . The second order model is given by the quadratic function $f_l(\sigma) = a_1 \sigma^2 + a_2 \sigma + a_3$ where σ is a coordinate along the $\mathbf{y}_{s+1} - \mathbf{y}_s$ direction. The coefficients a_1 , a_2 and a_3 are computed so that f_l interpolates the values $I_d(\mathbf{y}_s)$, $I_d(\mathbf{y}_{s+1})$ and $I_d(\mathbf{x}_{i,k})$. In particular, for $\sigma = 0$ $f_l = I_d(\mathbf{y}_s)$, for $\sigma = 1$ $f_l = I_d(\mathbf{y}_{s+1})$ and for

$\sigma = (\mathbf{x}_{i,k} - \mathbf{y}_s) / \|\mathbf{x}_{i,k} - \mathbf{y}_s\|$ $f_l = I_d(\mathbf{x}_{i,k})$. Then, a new sample \mathbf{y}_{s+2} is taken at the minimum of the second-order model along the $\mathbf{y}_{s+1} - \mathbf{y}_s$ direction.

Algorithm 2 Individual Actions in P_k^l

- 1: $s = 1, stop = 0$
 - 2: **if** $\mathbf{x}_{i,k} \prec \mathbf{x}_{i,k-1}$ **then**
 - $\mathbf{y}_s = \mathbf{x}_{i,k} + \bar{\lambda}(\mathbf{x}_{i,k} - \mathbf{x}_{i,k-1})$
 - with $\bar{\lambda} = \min\{1, \max\{\lambda : \mathbf{y}_s \in D\}\}$.
 - 3: **end if**
 - 4: **if** $\mathbf{x}_{i,k} \prec \mathbf{y}_s$ **then**
 - $s = s + 1$
 - $\mathbf{y}_s = \mathbf{e}[\mathbf{x}_{i,k} - (\mathbf{x}_{i_1,k} + (\mathbf{x}_{i_3,k} - \mathbf{x}_{i_2,k}))]$
 - $\forall j | y_s(j) \notin D, y_s(j) = r(b_u(j) - b_l(j)) + b_l(j)$,
 - with $j = 1, \dots, n$ and $r \in U(0, 1)$
 - 5: **else** $stop = 1$
 - 6: **end if**
 - 7: **if** $\mathbf{x}_{i,k} \prec \mathbf{y}_s$ **then**
 - $s = s + 1$
 - Generate $\mathbf{y}_s \in N_\rho(\mathbf{x}_{i,k})$.
 - Compute $\mathbf{y}_{s+1} = \mathbf{x}_{i,k} + \bar{\lambda}r^t(\mathbf{x}_{i,k} - \mathbf{y}_s)$
 - with $\bar{\lambda} = \min\{1, \max\{\lambda : \mathbf{y}_s \in D\}\}$
 - and $r \in U(0, 1)$.
 - Compute $\mathbf{y}_{s+2} = \bar{\lambda}\sigma_{min}(\mathbf{y}_{s+1} - \mathbf{y}_s) / \|(\mathbf{y}_{s+1} - \mathbf{y}_s)\|$,
 - with $\sigma_{min} = \arg \min_\sigma \{a_1\sigma^2 + a_2\sigma + I_d(\mathbf{y}_s)\}$,
 - and $\bar{\lambda} = \min\{1, \max\{\lambda : \mathbf{y}_{s+2} \in D\}\}$.
 - $s = s + 2$
 - 8: **else** $stop = 1$
 - 9: **end if**
 - 10: **Termination** Unless $s > s_{max}$ or $stop = 1$, GoTo Step 4
-

The position of $\mathbf{x}_{i,k}$ in D is then updated with the \mathbf{y}_s that has $I_d = 0$ and the longest vector difference in the criteria space with respect to $\mathbf{x}_{i,k}$. The displaced vectors \mathbf{y}_s generated by the agents in P_k^l are not discarded but contribute to a local archive A_l , one for each agent, except for the one selected to update the location of $\mathbf{x}_{i,k}$. In order to rank the \mathbf{y}_s , the following modified dominance index is used:

$$\hat{I}_d(\mathbf{x}_{i,k}) = \left| \{j \mid f_j(\mathbf{y}_s) = f_j(\mathbf{x}_{i,k})\} \right| \kappa + \left| \{j \mid f_j(\mathbf{y}_s) > f_j(\mathbf{x}_{i,k})\} \right| \quad (11)$$

where κ is equal to one if there is at least one component of $\mathbf{f}(\mathbf{x}_{i,k}) = [f_1, f_2, \dots, f_m]^T$ which is better than the corresponding component of $\mathbf{f}(\mathbf{y}_s)$, and is equal to zero other-

wise.

Now, if for the s^{th} outcome, the dominance index in Eq. (11) is not zero but is lower than the number of components of the objective vector, then the agent $\mathbf{x}_{i,k}$ is only partially dominating the s^{th} outcome. Among all the partially dominated outcomes with the same dominance index we select the one that satisfies the condition:

$$\min_s \langle (\mathbf{f}(\mathbf{x}_{i,k}) - \mathbf{f}(\mathbf{y}_s)), \mathbf{e} \rangle \quad (12)$$

where \mathbf{e} is the unit vector of dimension m , $\mathbf{e} = \frac{[1,1,1,\dots,1]^T}{\sqrt{m}}$. All the non-dominated and selected partially dominated solutions form the local archive A_l .

3.4. THE LOCAL AND GLOBAL ARCHIVES A_L AND A_G

Since the outcomes of one agent could dominate other agents or the outcomes of other agents, at the end of each generation, every A_l and the whole population P_k are added to the current global archive A_g . The global A_g contains X_k , the current best estimate of X_g . The dominance index in Eq.(3) is then computed for all the elements in $\hat{A}_g = A_g \cup_l A_l \cup P_k$ and only the non-dominated ones with crowding distance $\|\mathbf{x}_{i,k} - \mathbf{x}_{A_g}\| > w_c$ are preserved (where \mathbf{x}_{A_g} is an element of A_g).

3.4.1. Attraction

The archive A_g is used to direct the movements of those agents that are outside X_k . All agents, for which $I_d \neq 0$ at step k , are assigned the position of the elements in A_g and their inertia component is recomputed as:

$$\Delta_I = r(\mathbf{x}_{A_g} - \mathbf{x}_{i,k}) \quad (13)$$

More precisely, the elements in the archive are ranked according to their reciprocal distance or crowding factor. Then, every agent for which $I_d \neq 0$ picks the least crowded element \mathbf{x}_{A_g} not already picked by any other agent.

3.5. STOPPING RULE

The search is stopped when a prefixed number N_e of function evaluations is reached. At termination of the algorithm the whole final population is inserted into the archive A_g .

4. COMPARATIVE TESTS

The proposed optimization approach was implemented in a software code, in Matlab, called MACS. In previous works [8,9], MACS was tested on single objective optimization problems related to space trajectory design, showing good performances. In this work, MACS was tested at first on a number of standard problems, found in literature, and then on three typical space trajectory optimization problems.

This paper extends the results presented in Vasile and Zuiani (2010) [13] by adding a broader suite of algorithms for multiobjective optimization to the comparison and a different formulation of the performance metrics.

4.1. TESTED ALGORITHMS

MACS was compared against a number of state-of-the-art algorithms for multiobjective optimization. For this analysis it was decided to take the basic version of the algorithms that is available online. Further developments of the basic algorithms have not been considered in this comparison and will be included in future works. Note that, all the algorithms selected for this comparative analysis use Pareto dominance as selection criterion.

The tested algorithms are: NSGA-II [14], MOPSO [15], PAES [16] and MTS [17]. A short description of each algorithm with their basic parameters follows.

4.1.1. NSGA-II

The Non-Dominated Sorting Genetic Algorithm (NSGA-II) is a genetic algorithm which uses the concept of dominance class (or depth) to rank the population. A crowding factor is then used to rank the individuals within each dominance class. Optimiza-

tion starts from a randomly generated initial population. The individuals in the population are sorted according to their level of Pareto dominance with respect to other individuals. To be more precise, a fitness value equal to 1 is assigned to the non-dominated individuals. Non-dominated individuals form the first layer (or class). Those individuals dominated only by members of the first layer form the second one and are assigned a fitness value of 2, and so on. In general, for dominated individuals, the fitness is given by the number of dominating layers plus 1. A crowding factor is then assigned to each individual in a given class. The crowding factor is computed as the sum of the Euclidean distances, in criteria space, with respect to other individuals in the same class, divided by the interval spanned by the population along each dimension of the objective space. Inside each class, the individuals with the higher value of the crowding parameter obtain a better rank than those with a lower one.

At every generation, binary tournament selection, recombination, and mutation operators are used to create an offspring of the current population. The combination of the two is then sorted according to dominance first and then to crowding. The non-dominated individuals with lowest crowding factor are then used to update the population.

The parameters to be set are the size of the population, the number of generations, the crossover and mutation probability, p_c and p_m , and distribution indexes for crossover and mutation, η_c and η_m , respectively. Three different ratios between population size and number of generations were considered: 0.08, 0.33 and 0.75. The values p_c and p_m were set to 0.9 and 0.2 respectively and kept constant for all the tests. The values, 5, 10 and 20, were considered for η_c , while tests were run for values of η_m equal to 5, 25 and 50.

4.1.2. MOPSO

MOPSO is an extension of Particle Swarm Optimization (PSO) to multiobjective problems. Pareto dominance is introduced in the selection criteria for the candidate solutions to update the population. MOPSO features an external archive which stores all the non-dominated solutions and at the same time is used to guide the search process of the

swarm. This is done by introducing the possibility to direct the movement of a particle towards one of the less crowded solutions in the archive. The solution space is subdivided into hypercubes through an adaptive grid. The solutions in the external archive are thus reorganized in these hypercubes. The algorithm keeps track of the crowding level of each hypercube and promotes movements towards less crowded areas. In a similar manner, it also gives priority to the insertion of new non-dominated individuals in less crowded areas if the external archive has already reached its predefined maximum size. For MOPSO three different ratios between population size and number of generations were tested: 0.08 0.33 0.75. It was also tested with three different numbers of subdivisions of the solution space: 10, 30, and 50. The inertia component in the motion of the particles was set to 0.4 and the weights of the social and individualistic components were set to 1

4.1.3. PAES

PAES is a (1 + 1) Evolution Strategy with the addition of an external archive to store the current best approximation of the Pareto front. It adopts a population of only a single chromosome which, at every iteration, generates a mutated copy. The algorithm then preserves the non-dominated one between the parent and the candidate solution. If none of the two dominates the other, the algorithm then checks their dominance index with respect to the solutions in the archive. If also this comparison is inconclusive, then the algorithm selects the one which resides in the less crowded region of the objective space. To keep track of the crowding level of the objective space, the latter is subdivided in an n-dimensional grid. Every time a new solution is added to (or removed from) the archive, the crowding level of the corresponding grid cell is updated. PAES has two main parameters that need to be set, the number of subdivisions in the space grid and the mutation probability. Values of 1, 2 and 4 were used for the former and 0.6 0.8 and 0.9 were used for the latter.

4.1.4. MTS

MTS is an algorithm based on pattern search. The algorithm first generates a population of uniformly distributed individuals. At every iteration, a local search is performed by a subset of individuals. Three different search patterns are included in the local search: the first is a search along the direction of each decision variable with a fixed step length; the second is analogous but the search is limited to one fourth of all the possible search directions; the third one also searches along each direction but selects only solutions which are evenly spaced on each dimension within a predetermined upper bound and lower bound. At each iteration and for each individual, the three search patterns are tested with few function evaluations to select the one which generates the best candidate solutions for the current individual. The selected one is then used to perform the local search which will update the individual itself. The step length along each direction, which defines the size of the search neighbourhood for each individual, is increased if the local search generated a non-dominated child and is decreased otherwise. When the neighbourhood size reaches a predetermined minimum value, it is reset to 40% of the size of the global search space. The non-dominated candidate solutions are then used to update the best approximation of the global Pareto front. MTS was tested with a population size of 20, 40 and 80 individuals.

4.2. PERFORMANCE METRICS

Two metrics were defined to evaluate the performance of the tested multiobjective optimizers:

$$M_{spr} = \frac{1}{M_p} \sum_{i=1}^{M_p} \min_{j \in N_p} 100 \left\| \frac{\mathbf{f}_j - \mathbf{g}_i}{\mathbf{g}_i} \right\| \quad (14)$$

$$M_{conv} = \frac{1}{N_p} \sum_{i=1}^{N_p} \min_{j \in M_p} 100 \left\| \frac{\mathbf{g}_j - \mathbf{f}_i}{\mathbf{g}_j} \right\| \quad (15)$$

where M_p is the number of elements, with objective vector \mathbf{g} , in the true global Pareto front and N_p is the number of elements, with objective vector \mathbf{f} , in the Pareto front that a given algorithm is producing. Although similar, the two metrics are measuring two

different things: M_{spr} is the sum, over all the elements in the global Pareto front, of the minimum distance of all the elements in the Pareto front N_p from the the i^{th} element in the global Pareto front. M_{conv} , instead, is the sum, over all the elements in the Pareto front N_p , of the minimum distance of the elements in the global Pareto front from the i^{th} element in the Pareto front N_p .

Therefore, if N_p is only a partial representation of the global Pareto front but is a very accurate partial representation, then metric M_{spr} would give a high value and metric M_{conv} a low value. If both metrics are high then the Pareto front N_p is partial and poorly accurate. The index M_{conv} is similar to the mean Euclidean distance [15], although in M_{conv} the Euclidean distance is normalized with respect to the values of the objective functions, while M_{spr} is similar to the generational distance [18], although even for M_{spr} the distances are normalized.

Given n repeated runs of a given algorithm, we can define two performance indexes: $p_{conv} = P(M_{conv} < tol_{conv})$ or the probability that the index M_{conv} achieves a value less than the threshold tol_{conv} and $p_{spr} = P(M_{spr} < tol_{spr})$ or the probability that the index M_{spr} achieves a value less than the threshold tol_{conv} .

According to the theory developed in [7, 19], 200 runs are sufficient to have a 95% confidence that the true values of p_{conv} and p_{spr} are within a $\pm 5\%$ interval containing their estimated value.

Performance index (14) and (15) tend to uniformly weigh every part of the front. This is not a problem for index (14) but if only a relatively small portion of the front is missed the value of performance index (15) might be only marginally affected. For this reason, we slightly modified the computation of the indexes by taking only the M_P^* and N_P^* solutions with a normalised distance in criteria space that was higher than 10^{-3} .

The global fronts used in the three space tests were built by taking a selection of about 2000 equispaced, in criteria space, nondominated solutions coming from all the 200 runs of all the algorithms.

4.3. PRELIMINARY TEST CASES

For the preliminary tests, two sets of functions, taken from the literature [14, 15], were used and the performance of MACS was compared to the results in [14] and [15]. Therefore, for this set of tests, MTS was not included in the comparison. The function used in this section can be found in Table 1.

Table 1: Multiobjective test functions

The first three functions were taken from [15]. Test cases *Deb* and *Scha* are two examples of disconnected Pareto fronts, *Deb2* is an example of problem presenting multiple local Pareto fronts, 60 in this two dimensional case.

The last three functions are instead taken from [14]. Test case *ZDT2* has a concave Pareto front with a moderately high-dimensional search space. Test case *ZDT6* has a concave Pareto front but because of the irregular nature of f_1 there is a strong bias in the distribution of the solutions. Test case, *ZDT4*, with dimension 10, is commonly recognized as one of the most challenging problems since it has 21^9 different local Pareto fronts of which only one corresponds to the global Pareto-optimal front.

As a preliminary proof of the effectiveness of MACS, the average Euclidean distance of 500 uniformly spaced points on the true optimal Pareto front from the solutions stored in A_g by MACS was computed and compared to known results in the literature. MACS was run 20 times to have a sample comparable to the one used for the other algorithms. The global archive was limited to 200 elements to be consistent with [14]. The value of the crowding factor w_c , the threshold ρ_{tol} and the convergence ρ_{min} were kept constant to $1e-5$ in all the cases to provide good local convergence.

To be consistent with [15], on *Deb*, *Scha* and, *Deb2*, MACS was run respectively for 4000, 1200 and 3200 function evaluations. Only two agents were used for these lower dimensional cases, with $f_e = 1/2$. On test cases *ZDT2*, *ZDT4* and *ZDT6*, MACS was run for a maximum of 25000 function evaluations to be consistent with [14], with three agents and $f_e = 2/3$ for *ZDT2* and four agents and $f_e = 3/4$ on *ZDT4* and *ZDT6*.

The results on *Deb*, *Scha* and, *Deb2* can be found in Table 2, while the results on *ZDT2*, *ZDT4* and *ZDT6* can be found in 3.

On all the smaller dimensional cases MACS performs comparably to MOPSO and better than PAES. It also performs than NSGA-II on *Deb* and *Deb2*. On *Scha* MACS performs apparently worse than NSGA-II, although after inspection one can observe that all the elements of the global archive A_g belong to the Pareto front but not uniformly distributed, hence the higher value of the Euclidean distance. On the higher dimensional cases, MACS performs comparably to NSGA-II on *ZDT2* but better than all the others on *ZDT4* and *ZDT6*. Note in particular the improved performance on *ZDT4*.

Table 2: Comparison of the average Euclidean distances between 500 uniformly space points on the optimal Pareto front for various optimization algorithms: smaller dimension test problems.

Table 3: Comparison of the average Euclidean distances between 500 uniformly space points on the optimal Pareto front for various optimization algorithms: larger dimension test problems.

On the same six functions a different test was run to evaluate the performance of different variants of MACS. For all variants, the number of agents, f_e , w_c , ρ_{tol} and ρ_{min} was set as before, but instead of the mean Euclidean distance, the success rates p_{conv} and p_{spr} were measured for each variant. The number of function evaluations for *ZDT2*, *ZDT4*, *ZDT6* and *Deb2* is the same as before, while for *Scha* and *Deb* it was reduced respectively to 600 and 1000 function evaluations given the good performance of MACS already for this number of function evaluations. Each run was repeated 200 times to have good confidence in the values of p_{conv} and p_{spr} .

Four variants were tested and compared to the full version of MACS. Variant MACS no local does not implement the individualistic moves and the local archive, variant MACS $\rho = 1$ has no adaptivity on the neighborhood, its size is kept fixed to 1, variant MACS $\rho = 0.1$ has the size of the neighborhood fixed to 0.1, variant MACS no attraction has the attraction mechanisms not active.

The result can be found in Table 4. The values of tol_{conv} and tol_{spr} are respectively 0.001 and 0.0035 for *ZDT2*, 0.003 and 0.005 for *ZDT4*, 0.001 and 0.025 for *ZDT6*, 0.0012 and 0.035 for *Deb*, 0.0013 and 0.04 for *Scha*, 0.0015 and 0.0045 for *Deb2*. This thresholds were selected to highlight the differences among the various variants. The table shows that the adaptation mechanism is beneficial in some cases although, in others, fixing the value of ρ might be a better choice. This depends on the problem and a general rule is difficult to derive at present. Other adaptation mechanisms could further improve the performance.

The use of individualistic actions coupled with a local archive is instead fundamental, so is the use of the attraction mechanism. Note, however, how the attraction mechanism penalizes the spreading on biased problems like *ZDT6*, this is expected as it accelerates convergence.

Table 4: Comparison of different variants of MACS.

4.4. APPLICATION TO SPACE TRAJECTORY DESIGN

In this section we present the application of MACS to three space trajectory problems: a two-impulse orbit transfer from a Low Earth Orbit (LEO) to a high-eccentricity Molniya-like orbit, a three-impulse transfer from a LEO to Geostationary Earth Orbit (GEO) and a multi-gravity assist transfer to Saturn equivalent to the transfer trajectory of the Cassini mission. The first two cases are taken from the work of Minisci et al. [7]. In the two-impulse case, the spacecraft departs at time t_0 from a circular orbit around the Earth (the gravity constant is $\mu_E = 3.986010^5 \text{ km}^3\text{s}^{-2}$) with radius $r_0 = 6721$ km and at time t_f is injected into an elliptical orbit with eccentricity $e_T = 0.667$ and semimajor axis $a_T = 26610$ km. The transfer arc is computed as the solution of a Lambert's problem [20] and the objective functions are the transfer time $T = t_f - t_0$ and the sum of the two norms of the velocity variations at the beginning and at the end of the transfer arc Δv_{tot} . The objectives are functions of the solution vector $\mathbf{x} = [t_0 \ t_f]^T \in D \subset \mathbb{R}^2$ The search space D is defined by the following intervals $t_0 \in [0 \ 10.8]$, and $t_f \in [0.03 \ 10.8]$.

In the three-impulse case, the spacecraft departs at time t_0 from a circular orbit around the Earth with radius $r_0 = 7000$ km and after a transfer time $T = t_1 + t_2$ is injected into a circular orbit with radius $r_f = 42000$. An intermediate manoeuvre is performed at time $t_0 + t_1$ and at position defined in polar coordinates by the radius r_1 and the angle θ_1 . The objective functions are the total transfer time T and the sum of the three impulses Δv_{tot} . The solution vector in this case is $\mathbf{x} = [t_0, t_1, r_1, \theta_1, t_f]^T \in D \subset \mathbb{R}^5$. The search space D is defined by the following intervals $t_0 \in [0, 1.62]$, $t_1 \in [0.03, 21.54]$, $r_1 \in [7010, 105410]$, $\theta_1 \in [0.01, 2\pi - 0.01]$, and $t_2 \in [0.03, 21.54]$. The Cassini case consists of 5 transfer arcs connecting a departure planet, the Earth, to the destination planet, Saturn, through a sequence of swing-by's with the planets: Venus, Venus, Earth, Jupiter. Each transfer arc is computed as the solution of a Lambert's problem [21] given the departure time from planet P_i and the arrival time at planet P_{i+1} . The solution of the Lambert's problems yields the required incoming and outgoing velocities at each swing-by planet v_{in} and v_{out} . The swing-by is modeled through a linked-conic approximation with powered maneuvers [22], i.e., the mismatch between the required outgoing velocity v_{rout} and the achievable outgoing velocity v_{aout} is compensated through a Δv maneuver at the pericenter of the gravity assist hyperbola. The whole trajectory is completely defined by the departure time t_0 and the transfer time for each leg T_i , with $i = 1, \dots, 5$. The normalized radius of the pericenter $r_{p,i}$ of each swing-by hyperbola is derived a posteriori once each powered swing-by manoeuvre is computed. Thus, a constraint on each pericenter radius has to be introduced during the search for an optimal solution. In order to take into account this constraint, one of the objective functions is augmented with the weighted violation of the constraints:

$$f(\mathbf{x}) = \Delta v_0 + \sum_{i=1}^4 \Delta v_i + \Delta v_f + \sum_{i=1}^4 w_i (r_{p,i} - r_{pmin,i})^2 \quad (16)$$

for a solution vector $\mathbf{x} = [t_0, T_1, T_2, T_3, T_4, T_5]^T$. The objective functions are, the total transfer time $T = \sum_i^5 T_i$ and $f(\mathbf{x})$. The minimum normalized pericenter radii are $r_{pmin,1} = 1.0496$, $r_{pmin,2} = 1.0496$, $r_{pmin,3} = 1.0627$ and $r_{pmin,4} = 9.3925$. The

search space D is defined by the following intervals: $t_0 \in [-1000, 0]$ MJD2000, $T_1 \in [30, 400]$ d, $T_2 \in [100, 470]$ d, $T_3 \in [30, 400]$ d, $T_4 \in [400, 2000]$ d, $T_5 \in [1000, 6000]$ d. The best known solution for the single objective minimization of $f(\mathbf{x})$ is $f_{best} = 4.9307$ km/s, with $\mathbf{x}_{best} = [-789.753, 158.2993, 449.3859, 54.7060, 1024.5896, 4552.7054]^T$.

4.4.1. Test Results

For this second set of tests, each algorithm was run for the same number of function evaluations. In particular, consistent with the tests performed in the work of Minisci et al., [7] we used 2000 function evaluations for the two-impulse case and 30000 for the three-impulse case. For the Cassini case, instead, the algorithms were run for 180000, 300000 and 600000 function evaluations.

Note that the version of all the algorithms used in this second set of tests is the one that is freely available online, written in c/c++. We tried in all cases to stick to the available instructions and recommendations by the author to avoid any bias in the comparison.

The thresholds values for the two impulse cases was taken from [7] and is $tol_{conv} = 0.1$, $tol_{spr} = 2.5$. For the three-impulse case instead we considered $tol_{conv} = 5.0$, $tol_{spr} = 5.0$. For the Cassini case we used $tol_{conv} = 0.75$, $tol_{spr} = 5$, instead. These values were selected after looking at the dispersion of the results over 200 runs. Lower values would result in a zero value of the performance indexes of all the algorithms, which is not very significant for a comparison.

MACS was tuned on the three-impulse case. In particular, the crowding factor w_c , the threshold ρ_{tol} and the convergence ρ_{min} were kept constant to $1e-5$, which is below the required local convergence accuracy, while f_e and n_{pop} were changed. A value of $1e-5$ is expected to provide good local convergence and good density of the samples belonging to the Pareto front. Table 5 reports the value of performance indexes p_{conv} and p_{spr} over 200 runs of MACS with different settings. The index p_{spr} and the index p_{conv} have different, almost opposite, trends. However, it was decided to select the setting that provides the best convergence, i.e. $n_{pop} = 15$ and $f_e = 1/3$. This setting will be used for all the tests in this paper.

On top of the complete algorithm, two variants of MACS were tested: one without

individualistic moves and local archive, denoted as *no local* in the tables, and one with no attraction towards the global archive A_g , denoted as *no att* in the tables. Only these two variants are tested on these cases as they displayed the most significant impact in the previous standard test cases and more importantly were designed specifically to improve performances.

NSGA-II, PAES, MOPSO and MTS were tuned as well on the three-impulse case. In particular, for NSGA-II the best result was obtained for 150 individuals and can be found in Table 6. A similar result could be obtained for MOPSO, see Table 7. For MTS only the population was changed while the number of individuals performing local moves was kept constant to 5. The results of the tuning of MTS can be found in Table 9. For the tuning of PAES the results can be found in Table 8.

All the parameters tuned in the three impulse case were kept constant except for the population size of NSGA-II and MOPSO. The size of the population of NSGA-II and MOPSO was set to 100 and 40 respectively on the two impulse case and was increased with the number of function evaluations in the Cassini case. In particular for NSGA-II the following ratios between population size and number of function evaluations was used: 272/180000, 353/300000, 500/600000. For MOPSO the following ratios between population size and number of function evaluations was used: 224/180000, 447/300000, 665/600000. This might not be the best way to set the population size for these two algorithms but it is the one that provided better performance in these tests.

Note that the size of the global archive for MACS was constrained to be lower than the size of the population of NSGA-II, in order to avoid any bias in the computation of M_{spr} .

The performance of all the algorithms on the Cassini case can be found in Table 12 for a variable number of function evaluations.

Figure 2: Three-impulse test case: a) Complete Pareto front, b) close-up of the Pareto fronts

Table 5: Indexes p_{conv} and p_{spr} for different settings of MACS

Figure 3: Cassini test case: a) Complete Pareto front, b) close-up of the Pareto fronts

For the three-impulse case, MACS was able to identify an extended Pareto front (see Fig.2(a) and Fig. 2(b) where all the non-dominated solutions from all the 200 runs are compared to the global front), compared to the results in [7]. The gap in the Pareto front is probably due to a limited spreading of the solutions in that region. Note the cusp due the transition between the condition in which 2-impulse solutions are optimal and the condition in which 3-impulse solutions are optimal.

Table 11 summarizes the results of all the tested algorithms on the two-impulse case. The average value of the performance metrics is reported with, in brackets, the associated variance over 200 runs. The two-impulse case is quite easy and all the algorithms have no problems identifying the front. However, MACS displays a better convergence than the other algorithms while the spreading of MOPSO and MTS is superior to the one of MACS.

The three-impulse case is instead more problematic (see Table 10). NSGA-II is not able to converge to the upper-left part of the front and therefore the convergence is 0 and the spreading is comparable to the one of MACS. All the other algorithms perform poorly with a value of almost 0 for the performance indexes. This is mainly due to the fact that no one can identify the vertical part of the front.

Note that the long tail identified by NSGA-II is actually dominated by two points belonging to the global front (see 2(b)).

Table 12 reports the statistics for the Cassini problem. On top of the performance of the three variants tested on the other two problems, the table reports also the result for 10 agents and $f_e = 5$. For all numbers of function evaluations MACS has better spreading than NSGA-II because NSGA-II converges to a local Pareto front. Nonetheless NSGA-II displays a more regular behavior and a better convergence for low number of function evaluations although it never reaches the best front. The Pareto fronts are represented in Fig. 3(a) and Fig. 3(b) (even in this case the figures represent all the non-dominated solutions coming from all the 200 runs). Note that, the minimum f returned by MACS

is the best known solution for the single objective version of this problem (see [9]). All the other algorithms perform quite poorly on this case.

Of all the variants of MACS tested on these problems the full complete one is performing the best. As expected, in all three cases, removing the individualistic moves severely penalizes both convergence and spreading. It is interesting to note that removing the attraction towards the global front is also comparatively bad. On the two impulse case it does not impact the spreading but reduces the convergence, while on the Cassini case, it reduces mean and variance but the success rates are zero. The observable reason is that MACS converges slower but more uniformly to a local Pareto front.

Finally, it should be noted that mean and variance seem not to capture the actual performance of the algorithms. In particular they do not capture the ability to identify the whole Pareto front as the success rates instead do.

Table 6: NSGAI tuning on the 3-impulse case

Table 7: PAES tuning on the 3-impulse case

5. CONCLUSIONS

In this paper we presented a hybrid evolutionary algorithm for multiobjective optimization problems. The effectiveness of the hybrid algorithm, implemented in a code called MACS, was demonstrated at first on a set of standard problems and then its performance was compared against NSGA-II, PAES, MOPSO and MTS on three space trajectory design problems. The results are encouraging as, for the same computational effort (measured in number of function evaluations, MACS was converging more accu-

Table 8: MOPSO tuning on the 3-impulse case.

Table 9: MTS tuning on the 3-impulse

rately than NSGA-II on the two-impulse case and managed to find a previously undiscovered part of the Pareto front of the three-impulse case. As a consequence, on the three-impulse case, MACS, has better performance metrics than the other algorithms. On the Cassini case NSGA-II appears to converge better to some parts of the front although MACS yielded solutions with better f and identifies once more a part of the front that NSGA-II cannot attain. PAES and MTS do not perform well on the Cassini case, while MOPSO converges well locally but, with the settings employed in this study, yielded a very poor spreading.

From the experimental tests in this paper we can argue that the following mechanisms seem to be particularly effective: the use of individual local actions with a local archive as they allow the individuals to move towards and within the Pareto set; the use of an attraction mechanism as it accelerates convergence.

Finally it should be noted that all the algorithms tested in this study use the Pareto dominance as selection criterion. Different criteria, like the decomposition in scalar subproblems, can be equally implemented in MACS, without disrupting its working principles, and lead to different performance results.

ACKNOWLEDGEMENTS

The authors would like to thank Dr. Edmondo Minisci and Dr. Giulio Avanzini for the two and three impulse cases and the helpful advice.

REFERENCES

- [1] V. Coverstone-Carroll, J.W. Hartmann, and W.M. Mason. Optimal multi-objective low-thrust spacecraft trajectories. *Computer Methods in Applied Mechanics and Engineering*, 186:387–402, 2000.
- [2] B. Dachwald. Optimization of interplanetary solar sailcraft trajectories using evolutionary neurocontrol. *Journal of Guidance, and Dynamics*, February 2004.
- [3] S. Lee, P. von Allmen, W. Fink, A.E. Petropoulos, and R.J. Terrile. Multi-objective evolutionary algorithms for low-thrust orbit transfer optimization. In

- Proceedings of the Genetic and Evolutionary Computation Conference (GECCO 2005)*, Washington DC, USA, June 25–29 2005.
- [4] O. Schütze, M. M. Vasile, and C.A. Coello Coello. Approximate solutions in space mission design. In *Parallel Problem Solving from Nature (PPSN 2008)*, Dortmund, Germany, September 13–17 2008.
- [5] O. Schütze, M. Vasile, O. Junge, M. Dellnitz, and D. Izzo. Designing optimal low-thrust gravity-assist trajectories using space pruning and a multi-objective approach. *Engineering Optimization*, 41(2), February 2009.
- [6] M. Dellnitz, S. Ober-Bilbaum, M. Post, O. Schütze, and Bianca Thiere. A multi-objective approach to the design of low thrust space trajectories using optimal control. *Celestial Mechanics and Dynamical Astronomy*, 105(1), February 2009.
- [7] E. Minisci and G. Avanzini. Optimisation of orbit transfer manoeuvres as a test benchmark for evolutionary algorithms. In *Proceedings of the 2009 IEEE Congress on Evolutionary Computation (CEC2009)*, Trondheim, Norway, May 2009.
- [8] M. Vasile. A behavioral-based meta-heuristic for robust global trajectory optimization. In *Proceedings of the 2007 IEEE Congress on Evolutionary Computation (CEC2007)*, Singapore, September 2007.
- [9] M. Vasile and M. Locatelli. A hybrid multiagent approach for global trajectory optimization. *Journal of Global Optimization*, 44(4):461–479, August. 2009.
- [10] Oliver Schütze, Adriana Lara, Gustavo Sanchez, and Carlos A. Coello Coello. HCS: A new local search strategy for memetic multi-objective evolutionary algorithms. *IEEE Transactions on Evolutionary Computation* (to appear), 2010.
- [11] Q. Zhang and H. Li. Moea/d: A multiobjective evolutionary algorithm based on decomposition. *IEEE Transactions on Evolutionary Computation*, 11(6), November.

- [12] K.V. Price, R.M. Storn, and J.A. Lampinen. *Differential Evolution. A Practical Approach to Global Optimization*. Natural Computing Series. Springer, 2005.
- [13] M. Vasile and F. Zuiani. A hybrid multiobjective optimization algorithm applied to space trajectory optimization. In *Proceedings of the IEEE International Conference on Evolutionary Computation*, Barcelona, Spain, July 2010.
- [14] K. A. Deb, A. Pratap, and T. Meyarivan. Fast elitist multi-objective genetic algorithm: Nsga-ii. Kangal report no. 200001, KanGAL, 2000.
- [15] C. Coello and M. Lechuga. Mopso: A proposal for multiple objective particle swarm optimization. Technical report evocinv-01-2001., CINVESTAV. Instituto Politecnico Nacional. Col. San Pedro Zacatenco. Mexico., 2001.
- [16] J.D. Knowles and D.W. Corne. The pareto archived evolution strategy : A new baseline algorithm for pareto multiobjective optimisation. In *Proceedings of the IEEE International Conference on Evolutionary Computation*, Washington DC, US, 1999.
- [17] Lin-Yu Tseng and Chun Chen. Multiple trajectory search for multiobjective optimization. In *Proceedings of the IEEE International Conference on Evolutionary Computation*, Singapore, 25-28 September 2007.
- [18] D.A. Van Veldhuizen and G.B. Lamont. Evolutionary computation and convergence to a pareto front. In *Late Breaking papers at the Genetic Programming*, 1998.
- [19] M. Vasile, E. Minisci, and M. Locatelli. On testing global optimization algorithms for space trajectory design. In *AIAA/AAS Astrodynamics Specialists Conference*, Honolulu, Hawaii, USA, Aug 2008.
- [20] G. Avanzini. A simple lambert algorithm. *Journal of Guidance, Control, and Dynamics*, 31(6):1587–1594, Nov.–Dec. 2008.
- [21] R. Battin. *An Introduction to the Mathematics and Methods of Astrodynamics*. AIAA, 1999.

- [22] D. R. Myatt, V.M. Becerra, S.J. Nasuto, and J.M. Bishop. Global optimization tools for mission analysis and design. Final rept. esa ariadna itt ao4532/18138/04/nl/mv,call03/4101, ESA/ESTEC, 2004.

Table 10: Summary of metrics M_{conv} and M_{spr} , and associated performance indexes p_{conv} and p_{spr} , on the three impulse test cases.

Table 11: Metrics M_{conv} and M_{spr} , and associated performance indexes p_{conv} and p_{spr} , on the two impulse test cases.

Table 12: Metrics M_{conv} and M_{spr} , and associated performance indexes p_{conv} and p_{spr} , on the Cassini case.

NOMENCLATURE

A_g	global archive
A_l	local archive
a_T	semimajor axis
D	search space
e_T	eccentricity
f	cost function
f_e	fraction of the population doing local moves
I_d	dominance index
M_{conv}	convergence metrics
M_{spr}	spreading metrics
N_ρ	neighborhood of solution \mathbf{x}
N_e	maximum number of allowed function evaluations
n_{eval}	number of function evaluations
n_{pop}	population size
P_i	i -th planet
P_k	population at generation k
p_{conv}	percentage of success on convergence
p_{spr}	percentage of success on spreading
r	random number
r_p	pericentre radius
r_{pmin}	minimum pericentre radius
S	selection function
s	resource index
T	transfer time
t_0	departure time
t_i	manoeuvre time
t_f	final time
U	uniform distribution

\mathbf{u}	variation of the solution \mathbf{x}
X	Pareto optimal set
\mathbf{x}	solution vector
y	mutate individual
w_c	tolerance on the maximum allowable crowding

Greek symbols

Δv	variation of velocity
ρ	size of the neighborhood N_ρ
μ_E	gravity constant
θ_i	true anomaly of manoeuvre i

LIST OF TABLES

Table 1: Multiobjective test functions

<i>Scha</i>	$f_2 = (x - 5)^2$
$x \in [-5, 10]$	$f_1 = \begin{cases} -x & \text{if } x \leq 1 \\ -2 + x & \text{if } 1 < x < 3 \\ 4 - x & \text{if } 3 < x \leq 4 \\ -4 + x & \text{if } x > 4 \end{cases}$
<i>Deb</i>	$f_1 = x_1$
$x_1, x_2 \in [0, 1]$	$f_2 = (1 + 10x_2) \left[1 - \left(\frac{x_1}{1+10x_2} \right)^\alpha - \frac{x_1}{1+10x_2} \sin(2\pi qx_1) \right]$
$\alpha = 2; q = 4$	
<i>Deb2</i>	$f_1 = x_1$
$x_1 \in [0, 1]$	$f_2 = g(x_1, x_2)h(x_1, x_2); g(x_1, x_2) = 11 + x_2^2 - 10 \cos(2\pi x_2)$
$x_2 \in [-30, 30]$	$h(x_1, x_2) = \begin{cases} 1 - \sqrt{\frac{f_1}{g}} & \text{if } f_1 \leq g \\ 0 & \text{otherwise} \end{cases}$
<i>ZDT2</i>	$g = 1 + \frac{9}{n-1} \sum_{i=2}^n x_i$
$x_i \in [0, 1];$	$h = 1 - \left(\frac{f_1}{g} \right)^2$
$i = 1, \dots, n$	$f_1 = x_1; f_2 = gh$
$n = 30$	
<i>ZDT4</i>	$g = 1 + 10(n-1) + \sum_{i=2}^n [x_i^2 - 10 \cos(2\pi qx_i)];$
$x_1 \in [0, 1];$	$h = 1 - \sqrt{\frac{f_1}{g}}$
$x_i \in [-5, 5];$	$f_1 = x_1; f_2 = gh$
$i = 2, \dots, n$	
$n = 10$	
<i>ZDT6</i>	$g = 1 + 9 \sqrt[4]{\frac{\sum_{i=2}^n x_i}{n-1}}$
$x_i \in [0, 1];$	$h = 1 - \left(\frac{f_1}{g} \right)^2$
$i = 1, \dots, n$	$f_1 = 1 - \exp(-4x_1) \sin^6(6\pi x_1); f_2 = gh$
$n = 10$	

Table 2: Comparison of the average Euclidean distances between 500 uniformly space points on the optimal Pareto front for various optimization algorithms: smaller dimension test problems.

Approach	Deb2	Scha	Deb
MACS	1.542e-3 (5.19e-4)	3.257e-3 (5.61e-4)	7.379e-4 (6.36e-5)
NSGA-II	0.094644 (0.117608)	0.001594 (0.000122)	0.002536 (0.000138)
PAES	0.259664 (0.573286)	0.070003 (0.158081)	0.002881 (0.00213)
MOPSO	0.0011611 (0.0007205)	0.00147396 (0.00020178)	0.002057 (0.000286)

Table 3: Comparison of the average Euclidean distances between 500 uniformly space points on the optimal Pareto front for various optimization algorithms: larger dimension test problems.

Approach	ZDT2	ZDT4	ZDT6
MACS	9.0896e-4 (4.0862e-5)	0.0061 (0.0133)	0.0026 (0.0053)
NSGA-II	0.000824 ($<1e-5$)	0.513053 (0.118460)	0.296564 (0.013135)
PAES	0.126276 (0.036877)	0.854816 (0.527238)	0.085469 (0.006644)

Table 4: Comparison of different versions of MACS.

Approach	Metric	ZDT2	ZDT4	ZDT6	Scha	Deb	Deb2
MACS	p_{conv}	83.5%	75%	77%	73%	70.5%	60%
	p_{spr}	22.5%	28%	58.5%	38.5%	83%	67.5 %
MACS no local	p_{conv}	14%	0%	45%	0.5%	72.5%	11%
	p_{spr}	1%	0%	34%	0%	4%	15%
MACS $\rho = 1$	p_{conv}	84%	22%	78%	37%	92%	21%
	p_{spr}	22%	7%	63%	0%	54%	38%
MACS $\rho = 0.1$	p_{conv}	56%	42%	57%	78%	85%	42%
	p_{spr}	5%	15%	61%	88%	94.5%	74%
MACS no attraction	p_{conv}	21%	0.5%	14.5%	0.5%	88.5%	0%
	p_{spr}	0%	0.5%	78.5%	0%	0%	0%

Table 5: Indexes p_{conv} and p_{spr} for different settings of MACS on the 3-impulse case

p_{conv}	$n_{pop} = 5$	$n_{pop} = 10$	$n_{pop} = 15$
$f_e = 1/3$	45.5%	55.5%	61.0%
$f_e = 1/2$	48.0%	51.0%	55.5%
$f_e = 2/3$	45.0%	52.5%	43.0%
p_{spr}	$n_{pop} = 5$	$n_{pop} = 10$	$n_{pop} = 15$
$f_e = 1/3$	68.5%	62.0%	56.0%
$f_e = 1/2$	65.0%	57.0%	46.0%
$f_e = 2/3$	67.5%	51.0%	36.5%

Table 6: NSGAI tuning on the 3-impulse case

Mean M_{conv}				Var M_{conv}			
η_c/η_m	5	25	50	η_c/η_m	5	25	50
5	36.1	38.3	43.0	5	201.0	202.0	185.0
10	32.3	39.4	40.6	10	182.0	172.0	182.0
20	31.7	39.6	42.5	20	175.0	183.0	169.0
Mean M_{spr}				Var M_{spr}			
η_c/η_m	5	25	50	η_c/η_m	5	25	50
5	6.77	7.24	8.08	5	9.97	9.47	7.25
10	5.91	7.50	7.81	10	9.74	8.68	8.34
20	5.78	7.50	8.16	20	9.75	8.53	8.04
p_{conv}				p_{spr}			
η_c/η_m	5	25	50	η_c/η_m	5	25	50
5	0.0%	0.0%	0.0%	5	44.8%	37.7%	23.4%
10	0.0%	0.0%	0.0%	10	57.8%	33.1%	29.2%
20	0.0%	0.0%	0.0%	20	61.0%	32.5%	24.7%

Table 7: MOPSO tuning on the 3-impulse case.

Mean M_{conv}				Var M_{conv}			
Particles/Subdivisions	10	30	50	Particles/Subdivisions	10	30	50
50	59.1	50.2	41.5	50	1080.0	1010.2	713.3
100	50.0	43.3	41.3	100	591.0	721.1	778.1
150	47.8	41.4	39.4	150	562.1	550.2	608.2
Mean M_{spr}				Var M_{spr}			
Particles/Subdivisions	10	30	50	Particles/Subdivisions	10	30	50
50	16.1	13.5	12.3	50	41.3	37.3	24.0
100	14.7	12.2	11.6	100	32.8	25.8	24.5
150	14.8	11.9	11.4	150	30.0	22.2	22.5
p_{conv}				p_{spr}			
Particles/Subdivisions	10	30	50	Particles/Subdivisions	10	30	50
50	0%	0%	0%	50	0.5%	2.5%	3.5%
100	0%	0%	0%	100	0.5%	4.5%	4%
150	0%	0%	0%	150	0.5%	2%	4%

Table 8: PAES tuning on the 3-impulse case

Mean M_{conv}				Var M_{conv}			
Subdivisions/Mutation	0.6	0.8	0.9	Subdivisions/Mutation	0.6	0.8	0.9
1	53.7	70.6	70.2	1	525.0	275.0	297.0
2	52.8	70.2	70.0	2	479.0	266.0	305.0
4	53.0	70.2	70.1	4	453.0	266.0	311.0
Mean M_{spr}				Var M_{spr}			
Subdivisions/Mutation	0.6	0.8	0.9	Subdivisions/Mutation	0.6	0.8	0.9
1	14.2	27.7	36.7	1	20.0	14.3	17.3
2	13.6	27.6	36.6	2	17.5	14.6	16.8
4	13.8	27.7	36.6	4	17.2	15.8	17.0
p_{conv}				p_{spr}			
Subdivisions/Mutation	0.6	0.8	0.9	Subdivisions/Mutation	0.6	0.8	0.9
1	0.0%	0.0%	0.0%	1	0.0%	0.0%	0.0%
2	0.0%	0.0%	0.0%	2	0.0%	0.0%	0.0%
4	0.0%	0.0%	0.0%	4	0.0%	0.0%	0.0%

Table 9: MTS tuning on the 3-impulse

3imp	Population	20	40	80
M_{conv}	Mean	17.8	22.6	23.6
	Var	97.6	87.8	73.2
M_{spr}	Mean	12.6	19.9	18.4
	Var	34.7	26.2	18.6
	p_{conv}	1.0%	0.0%	0.0%
	p_{spr}	0.5%	0.0%	0.0%

Table 10: Summary of metrics M_{conv} and M_{spr} , and associated performance indexes p_{conv} and p_{spr} , on the three impulse test cases.

Metric	MACS	MACS no local	MACS no att	NSGA-II	PAES	MOPSO	MTS
M_{conv}	5.53 (15.1)	7.58 (26.3)	154.7 (235.0)	31.7 (175.0)	53.0 (453.0)	39.4 (608.1)	17.8 (97.6)
M_{spr}	5.25 (3.73)	6.03 (3.95)	9.16 (2.07)	5.78 (9.75)	13.8 (17.2)	11.4 (22.5)	12.6 (34.7)
p_{conv}	61.0%	40.5%	0.0%	0.0%	0.0%	0%	1.0%
p_{spr}	56.0%	36%	0.0%	61.0%	0.0%	4.0%	0.5%

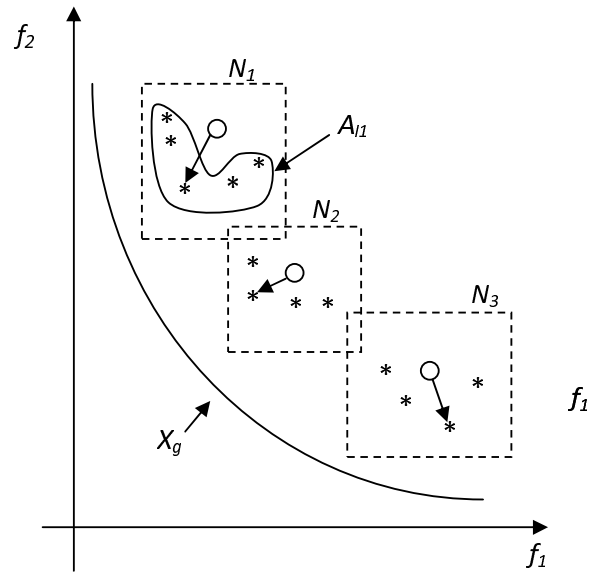
Table 11: Metrics M_{conv} and M_{spr} , and associated performance indexes p_{conv} and p_{spr} , on the two impulse test cases.

Metric	MACS	MACS no local	MACS no att	NSGA-II	PAES	MOPSO	MTS
M_{conv}	0.0077 (1e-3)	0.0039 (1.4e-2)	0.0534 (9.5e-3)	0.283 (4.35e-3)	0.198 (0.332)	0.378 (0.0636)	0.151 (0.083)
M_{spr}	2.89 (0.49)	6.87 (7.36)	3.08 0.943	2.47 (0.119)	332.0 (2.61e4)	2.11 (2.65)	1.95 (1.41)
p_{conv}	98.5%	91.5%	84%	0%	75.5%	9%	57.5%
p_{spr}	29.5%	0%	24%	62.5%	0.5%	94.5%	85.5%

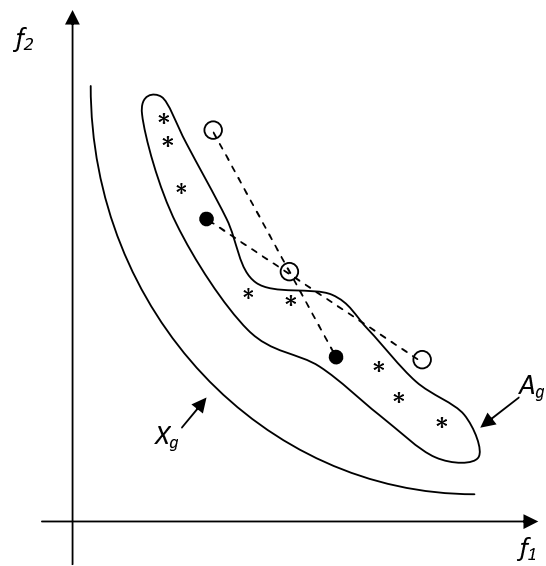
Table 12: Metrics M_{conv} and M_{spr} , and associated performance indexes p_{conv} and p_{spr} , on the Cassini case.

Approach	Metric	180k	300k	600k
MACS 5/15	M_{conv}	6.50 (229.1)	4.48 (107.1)	3.91 (62.6)
	M_{spr}	12.7 (126.0)	11.1 (83.1)	8.64 (35.5)
	p_{conv}	6%	14%	21.5%
	p_{spr}	27.5%	31%	41%
MACS 5/10	M_{conv}	6.74 (217.9)	5.56 (136.4)	3.14 (50.1)
	M_{spr}	12.1 (83.0)	10.3 (63.7)	8.11 (30.0)
	p_{conv}	8%	10%	25.5%
	p_{spr}	26.0%	31.5%	45.5%
MACS no local	M_{conv}	13.5 (436.2)	10.2 (350.1)	7.86 (190.2)
	M_{spr}	31.1 (274.3)	27.9 (278.9)	21.9 (226.7)
	p_{conv}	1.0%	1.5%	2.5%
	p_{spr}	1.0%	2.5%	6%
MACS no att	M_{conv}	2.62 (1.46)	2.2 (0.88)	1.82 (0.478)
	M_{spr}	27.8 (83.2)	22.9 (58.0)	18.2 (28.0)
	p_{conv}	0.0%	0.0%	1.0%
	p_{spr}	0.0%	0.0%	0.0%
NSGA-II	M_{conv}	2.43 (18.0)	1.99 (16.8)	1.24 (1.62)
	M_{spr}	11.6 (71.4)	11.0 (47.5)	8.78 (28.2)
	p_{conv}	17.5%	24.0%	29.0%
	p_{spr}	15.5%	12.5%	25.0%
MOPSO	M_{conv}	2.62 (7.33)	2.4 (2.57)	2.14 (0.94)
	M_{spr}	28.0 (308.3)	24.6 (260.4)	21.8 (231.3)
	p_{conv}	0.5%	1.0%	1.0%
	p_{spr}	0.0%	0.0%	0.5%
PAES	M_{conv}	24.0 (54.5)	19.8 (32.9)	15.2 (16.6)
	M_{spr}	30.1 (47.3)	26.0 (33.9)	21.4 (19.5)
	p_{conv}	0.0%	0.0%	0.0%
	p_{spr}	0.0%	0.0%	0.0%
MTS	M_{conv}	3.71 (1.53)	3.39 (1.67)	3.02 (1.69)
	M_{spr}	18.1 (18.2)	15.6 (13.4)	13.1 (8.46)
	p_{conv}	0.0%	0.0%	0.0%
	p_{spr}	0.0%	0.0%	0.0%

LIST OF FIGURES

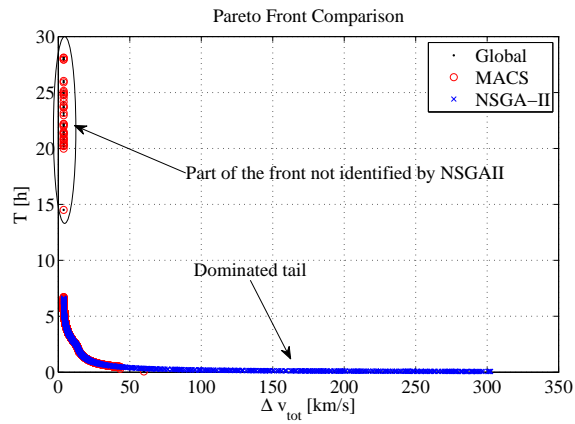
f_1 

(a)

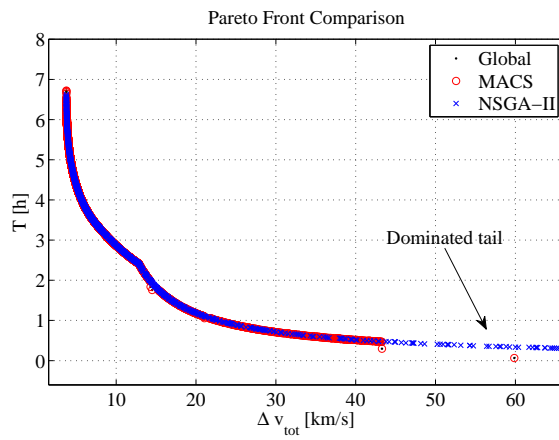


(b)

Figure 1: Illustration of the a) local moves and archive and b) global moves and archive.

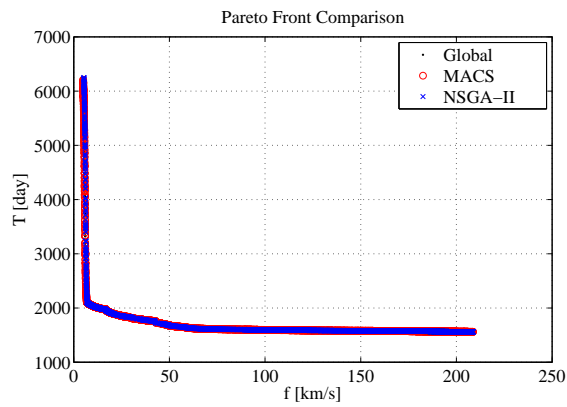


(a)

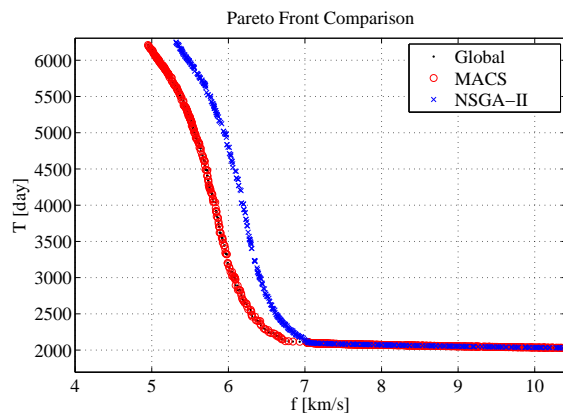


(b)

Figure 2: Three-impulse test case: a) Complete Pareto front, b) close-up of the Pareto fronts



(a)



(b)

Figure 3: Cassini test case: a) Complete Pareto front, b) close-up of the Pareto fronts

Pareto Front Comparison

